Physica 16D (1985) 233–242
North-Holland, Amsterdam

CHAOS IN A THREE-VARIABLE MODEL OF AN EXCITABLE CELL†

Teresa Ree CHAY
Department of Biological Sciences, University of Pittsburgh, Pittsburgh, PA 15260, USA

Received 17 September 1984

We describe chaotic behavior in a model that consists of three first-order, non-linear differential equations, which represent ionic events in excitable membranes. For a certain range of conductances, the model generates chaotic action potentials, and the intracellular calcium concentration also varies chaotically. The chaos was characterized by constructing phase portraits and one-variable maps using the membrane potentials and calcium concentrations. This is the first, simple, biophysically realistic model for excitable cells that shows endogenous chaos.

1. Introduction

The transition from periodic to aperiodic dynamics has attracted many physicists, chemists, biologists, and mathematicians in recent years [1–7]. There are many fascinating examples of chaos in biological systems [1–3, 5, 8–10, 13–17]. Chaos has been demonstrated, both experimentally and theoretically, in excitable membrane systems driven by a periodic external current [3, 5, 9]. There have also been some systematic identification of chaos in models for non-driven (endogenous) electrically excitable cardiac cells [13], neurons [14] and β-cells of the pancreas [16]. These models contain at least five differential equations. The aims of this note are, first, to present a unified model for both the neuronal and secretory excitable membranes that contains just three dynamic variables, and second, to show that this simple system exhibits period doubling and chaos even in the absence of an externally driven rhythm.

†This work was supported by NSF PCM82 15583.

2. Model

As in the Plant model [18] as well as in the Chay model [19] of neurons, and in the Chay–Keizer model of pancreatic β-cell [20], an excitable membrane is considered to contain voltage-sensitive channels which allow Na^+ and Ca^{2+} ions to enter the cell, voltage-sensitive K^+-channels which allow K^+ ions to leave, and voltage-insensitive K^+-channels known to be activated by intracellular calcium ions [21]. The current is the product of a conductance and a driving force, the difference between the membrane potential and the reversal potential for the conductance.

Thus, there are two types of currents passing through the membrane: the outward current carried by K^+ ions passing through the voltage- and Ca-sensitive channels and the inward current carried by Na^+ and Ca^{2+} passing through the voltage-sensitive Na^+ and Ca^{2+} channels. In the β-cells the voltage-sensitive Na^+ conductance is almost inactive, and thus the inward current is almost exclusively carried by Ca^{2+} ions through the voltage-sensitive Ca^{2+} channel [21]. In neuro-

nal cells, however, the inward current is carried by Na^+ as well as Ca^{2+} ions through two separate channels that differ in their selectivity and kinetics [22, 23]. Nevertheless, the use of a "mixed effective" reversal potential has proven to be convenient in previous studies [18, 24]. The assumption of a "mixed" effective conductance [25] should not affect the results, and thus we formulate our mathematical model by expressing the total inward current in terms of a single mixed conductance g_I and reversal potential V_I to represent the effect of the two functionally independent Na^+ and Ca^{2+} channels.

In terms of a Hodgkin–Huxley type formalism [26] the dynamics of the membrane potential V of such a system may be written as

$$dV/dt = g_I^* m_\infty^3 h_\infty (V_I - V) + g_{K,V}^* n^4 (V_K - V) + g_{K,C}^* \frac{C}{1+C}(V_K - V) + g_L^* (V_L - V). \quad (1)$$

Here, V_I, V_K, and V_L are the reversal potentials for "mixed" Na^+–Ca^{2+}, K^+, and leakage ions, respectively; C is the concentration of intracellular Ca^{2+} ions divided by its dissociation constant from the receptor; g_I^*, $g_{K,V}^*$, $g_{K,C}^*$, and g_L^* are the maximal conductances divided by the membrane capacitance, where the subscripts I, (K, V), (K, C), and (L) refer to the voltage-sensitive mixed ion channel, voltage-sensitive K^+ channel, Ca^+-sensitive K^+ channel, and the leakage channels, respectively.

In eq. (1), m_∞ and h_∞ are the probabilities of activation and inactivation of the mixed channel. The probability n of opening the voltage-sensitive K^+-channel is a dynamic variable, which is assumed to follow first-order kinetics [26]:

$$dn/dt = [n_\infty - n]/\tau_n. \quad (2)$$

where τ_n is the relaxation time (in s), and n_∞ is the steady state value of n. Note in eq. (1) that the usual time dependencies of m and h in the Hodgkin–Huxley equations are replaced by their respective steady state values in our formulation. This is because the relaxation time for the mixed conductance is so small that such a replacement does not affect the results (while saving greatly on computation time)†. Explicit expressions for m_∞, h_∞, n_∞, and τ_n are given in the Appendix.

The dynamics of the intracellular free calcium concentration depend on the inward calcium current and sequestration of intracellular Ca^{2+} ions by the intracellular compartments [18–20]. Thus, using the rate law the time derivative of C may be expressed by

$$dC/dt = \rho \{ m_\infty^3 h_\infty (V_C - V) - k_C C \}, \quad (3)$$

where k_C is the rate constant for the efflux of intracellular Ca^{2+} ions, ρ is a proportionality constant, and V_C the reversal potential for Ca^{2+} ions.

As described above, our excitable cell model consists of first-order, non-linear equations with the following three dynamic variables: (i) the membrane potential, V, whose variation with time is expressed as the sum of ionic currents carried by outward K^+ ions and inward Na^+/Ca^{2+} ions and the leakage current of an unspecified nature; (ii) the probability, n, of opening the voltage-dependent K^+ channel; (iii) C, the intracellular concentration of Ca^{2+} ions.

3. Solution and results

We have solved eqs. (1), (2), and (3) numerically in double precision on a DEC 10 computer using a Gear algorithm, with absolute and relative error tolerances set at 10^{-10}. The parameter values used for our computations are listed in the fig. 1 caption.

The following quantities were obtained by numerical solutions to demonstrate the deterministic nature of chaos in the model: (i) the dynamics

†Rinzel [27] has found that for some parameter ranges many features of the Hodgkin–Huxley dynamics are reproduced quantitatively with two dynamic variables where $m = m_\infty$ and n as a function of h.

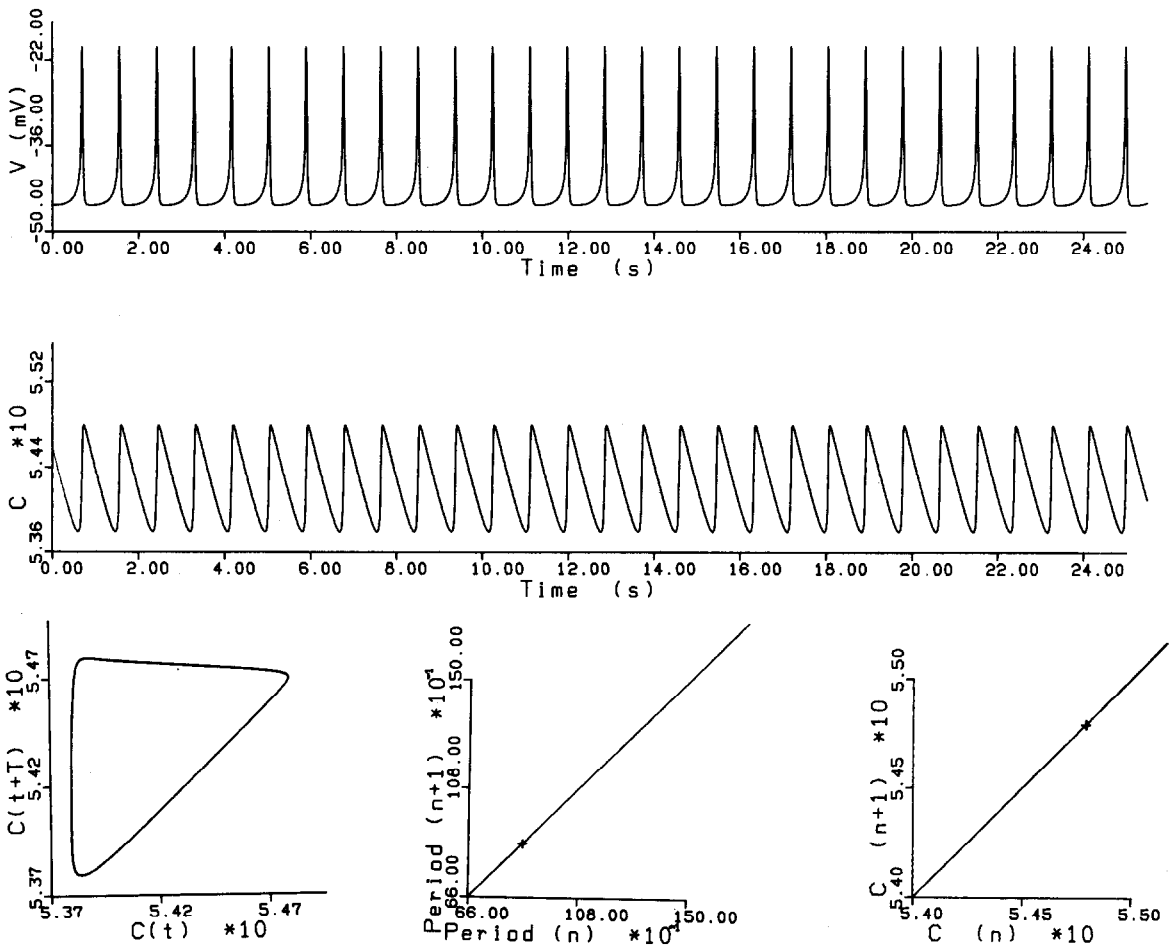

Fig. 1. Periodic repetitive firing of the excitable cell at $g^*_{K,C} = 10\ s^{-1}$. The top row shows the time sequence of membrane potentials; the middle row that of calcium concentration; the bottom row the traejectories of C at time t vs. that at time $t + 75$ ms (left); the one-dimensional map constructed from the spike-to-spike interval lengths (middle); the one-dimensional map constructed from the successive local maxima of calcium concentrations (right). The values of the parameters used in this figure and the subsequent figures are: $V_K = -75$ mV, $V_I = 100$ mV, $V_L = -40$ mV, $V_C = 100$ mV, $V_n = -30$ mV, $V_m = -50$ mV, $g^*_{K,V} = 1700\ s^{-1}$, $g^*_I = 1800\ s^{-1}$, $g^*_L = 7\ s^{-1}$, $k_C = 3.3/18$ mV, and $\rho = 0.27\ mV^{-1}\ s^{-1}$.

of membrane potentials, which reveal the transition from a regular mode to a non-periodic (chaotic) mode; (ii) the variation of C with time, which closely follows the mode of the potentials; (iii) phase portraits, constructed from the intracellular calcium concentration, which reveal the chaotic paths; (iv) limit cycles constructed from the membrane potential and C; and finally (v) one-dimensional maps, which confirm that the irregular characteristic of the action potentials is indeed deterministic in nature. All these quantities are not only very useful in determining the chaotic nature of the irregularity, but they can also be compared directly to experimental measurements.

Figs. 1–5 show various modes of the oscillatory patterns obtained as $g^*_{K,C}$, the maximal conductance of the Ca^{2+}-sensitive K^+-channel, is increased from 10 s^{-1} to 11.5 s^{-1}. We show in the first two rows the time sequences of membrane potentials and intracellular calcium concentrations. Note that when $g^*_{K,C} = 10\ s^{-1}$ the cell fires repetitive action potentials at a regular interval

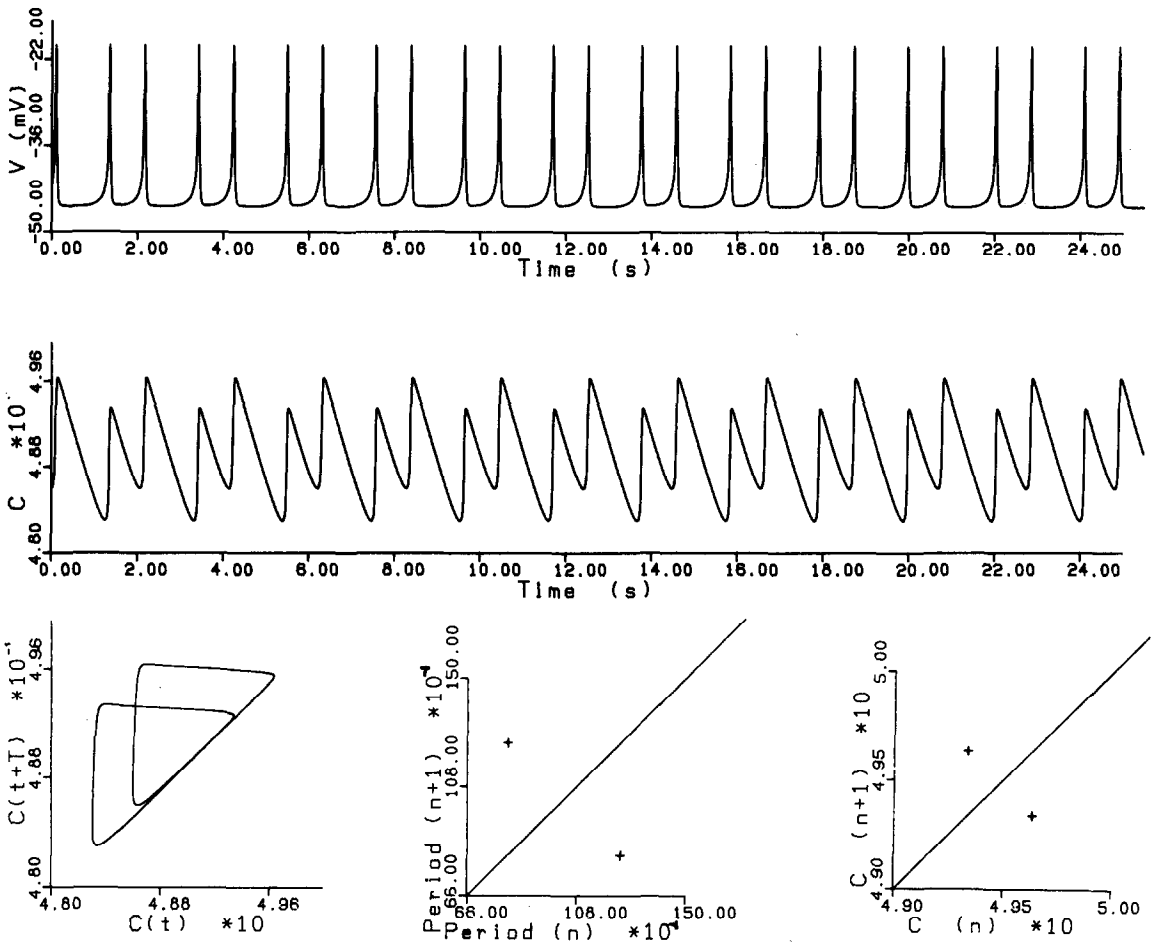

Fig. 2. Doublets in action potentials and other quantities when $g^*_{K,C}$ was increased to 10.7 s^{-1}.

(see fig. 1). Note also in fig. 5 that when $g^*_{K,C} = 11.5$ s^{-1} the same cell fires bursts of several action potentials, and each cluster of V pulses is separated by an interval of quiescence. During the active phase $[Ca^{2+}]_i$ increases with individual action potentials, and in the quiet intervals it falls to its minimum value. This is consistent with experimental simultaneous recordings of membrane potential and absorbance changes (which monitor intracellular Ca^{2+} activity) from an arsenazo III-injected Apylsia neuron [28]. Note that the membrane potentials in figs. 1–5 show regular, patterned, irregular and bursting discharges similar to those observed in neurons [29–31].

Period doubling can be observed as repetitive doublet pulses separated by quiet periods of V (see figs. 2 and 3). For intermediate values of $g^*_{K,C}$, we find chaos (fig. 4). The change in patterning from a regular to doublet discharge is more apparent in $C(t)$ than $V(t)$. The development of chaos and period doubling can be seen more clearly from the phase portrait and one-dimensional maps in the bottom traces of figs. 1–5. In the left column of the bottom row, we show trajectories of $C(t)$ versus $C(t+\tau)$. This phase portrait was constructed by placing the calcium concentration at time t on the x-axis and its value after a delay of 75 ms on the y-axis. The one-variable map in the

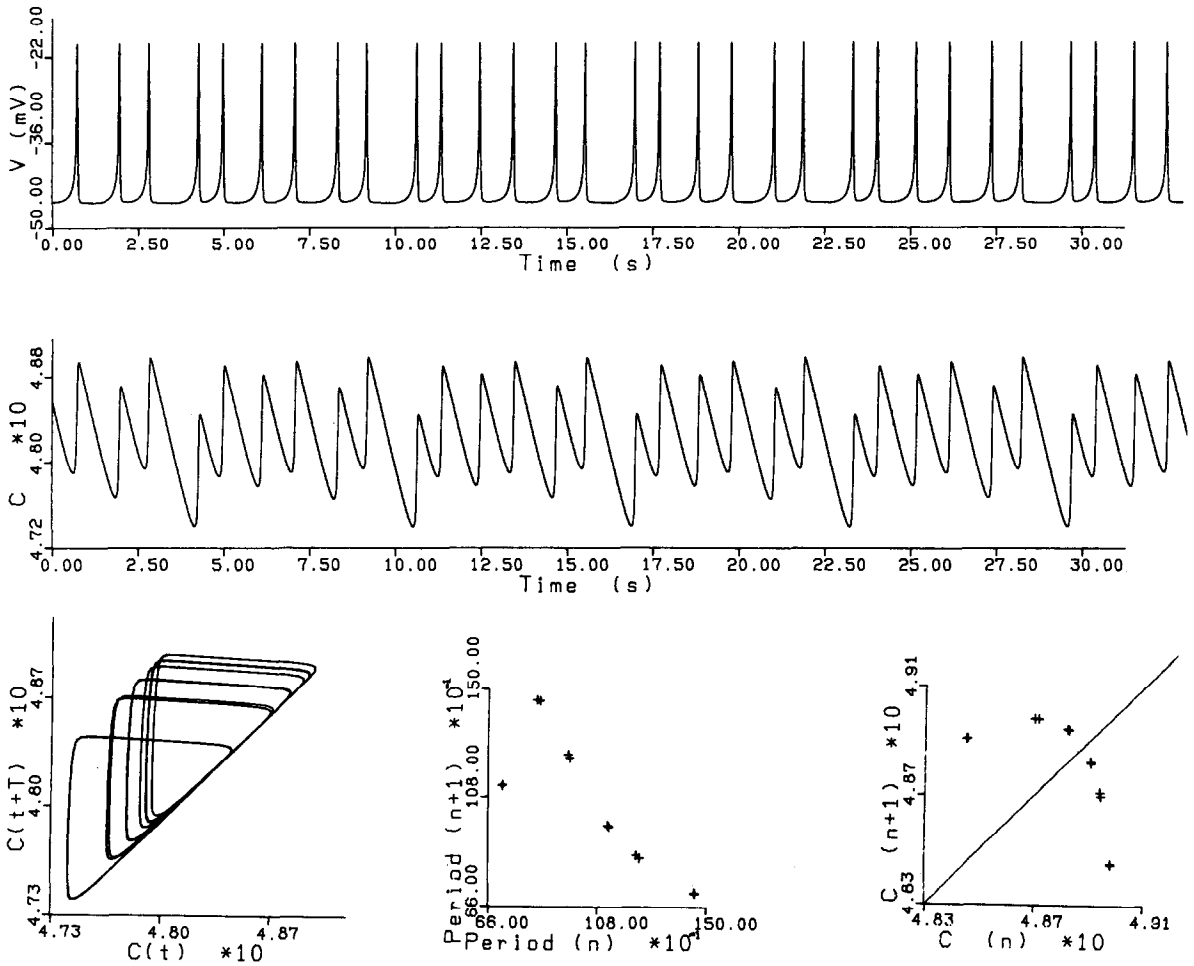

Fig. 3. Period of 12 when $g^*_{K,C}$ was increased to 10.8 s^{-1}.

middle column of the bottom traces describes the evolution of the interspike width T_n (in ms between the nth and $n+1$st spike) to T_{n+1} (i.e., that between $n+1$st and $n+2$nd) [16]. In the right-hand column, we present one-dimensional maps constructed from the relative maxima of calcium concentrations. Note from fig. 4 that the one-dimensional maps generated from the mode resemble those generated from first-order, non-linear dynamic equations [1] and from the experiment of Belousov–Zhabotinskii reaction [4], in exhibiting a unimodal hump.

Now, let us examine these maps closely. As $g^*_{K,C}$ is increased from 10 s^{-1} we see a period-doubling sequence; i.e., 2τ at $g^*_{K,C} = 10.7$, 4τ at 10.75, 8τ at 10.77, and 12τ at 10.8 (4τ and 8τ not shown here). At the point crossing the 1:1 line (i.e., the fixed point) the slope becomes steeper than -1 with increasing $g^*_{K,C}$, and hence the system becomes unstable when $g^*_{K,C}$ is larger than 10.7. As the system becomes unstable, the oscillatory behavior goes from a stable point, through a bifurcating hierarchy of stable cycles of 2^n periods, into a region of chaotic behavior. But, as $g^*_{K,C}$ increases beyond 11.3 we begin to see rhythmic bursting (see fig. 5). When $g^*_{K,C}$ is not very high (i.e., about 11.5), there are several successive increases before the calcium concentration falls again

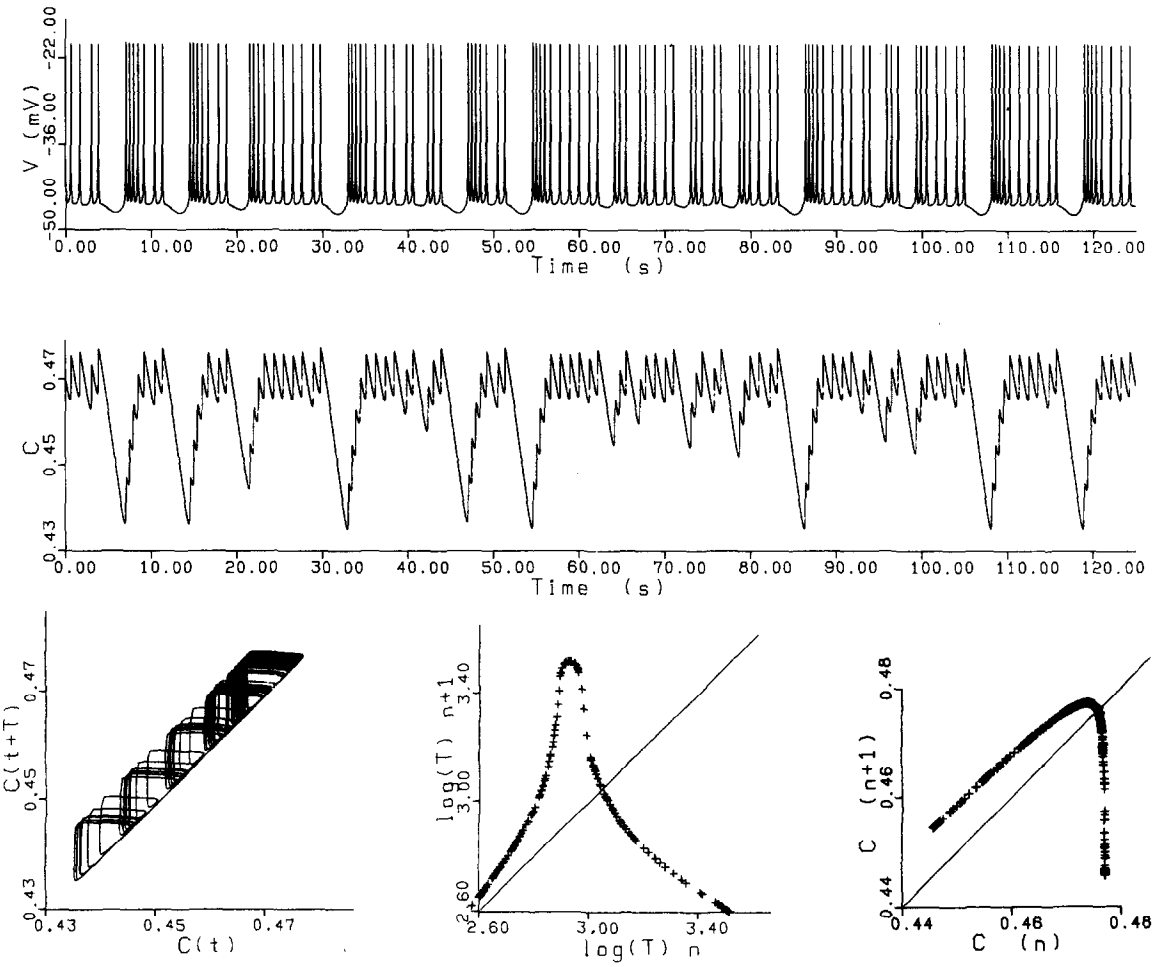

Fig. 4. Aperiodic chaos when $g^*_{K,C}$ was increased further to 11 s^{-1}.

(see fig. 5). As $g^*_{K,C}$ becomes very large, however, the attractors which lie on the left side of the 1:1 line move farther away from this line. This would yield fewer pulses per burst, i.e., larger increment in C per spike (see fig. 7).

To show how the periodic and aperiodic states develop from the stable steady state and are lost as $g^*_{K,C}$ changes, we have constructed a bifurcation diagram, and this is presented in fig. 6. AUTO, a program for the automatic bifurcation analysis developed by Doedel (32), was used to construct fig. 6. This AUTO analyzer computes the regions of the periodic branches, steady state branches, Hopf bifurcation points, as well as the period in the periodic branches, as shown in this figure. Here, the top row shows the membrane potential as a function of $g^*_{K,C}$; the middle row the intracellular calcium concentration C against $g^*_{K,C}$; the last row its period. Note that there are two Hopf bifurcation points (HB); one at -7.790 s^{-1} (its membrane potential at -26.76 mV) and another one at 27.25 s^{-1} ($V = 47.53$ mV). The existence of two bifurcation points implies that the stable steady state exists in the interval between $-\infty$ and -7.79 and another one between 27.25 and $+\infty$ and that the periodic state exists between -7.79 and 27.25. Negative values of conductance have no physical significance. A discontinuity seen

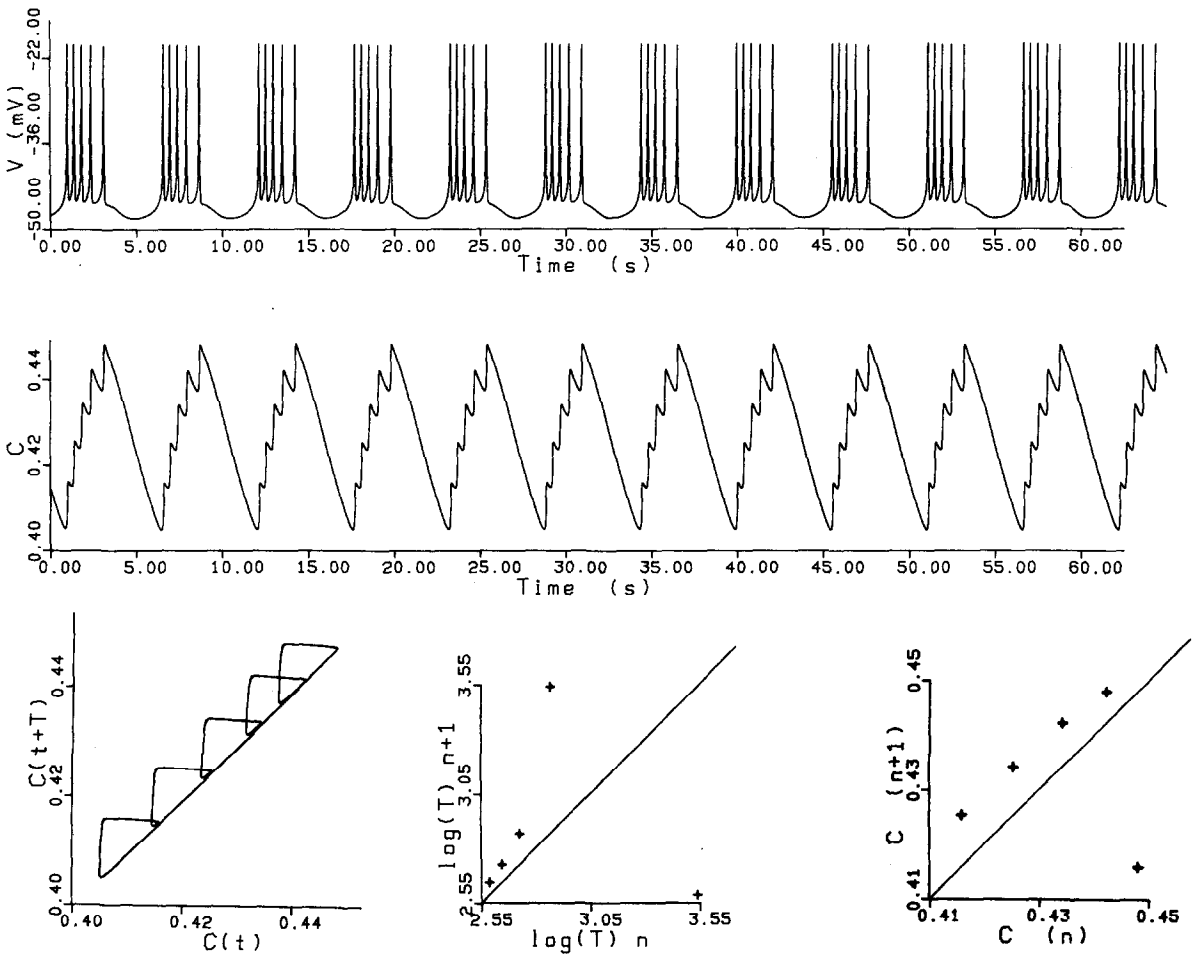

Fig. 5. Regular bursting of the same cell when $g^*_{K,C}$ was increased to 11.5 s^{-1}.

in the periodic state between $g^*_{K,C} = 19$ and 27 s^{-1} is that a bifurcating hierarchy of stable and unstable cycles arises as $g^*_{K,C}$ enters into the bursting region, and therefore it would take an excessive computer time to search for a succession of pitchfork bifurcations. For the same reason, we were unable to find all the stable and unstable fixed points of 2^n periods, which arise in the region between ~ 10.7 and ~ 10.8 s^{-1}. Our dynamic solution indicates that the chaotic region exists between ~ 10.9 and ~ 11.3 s^{-1}.

As $g^*_{K,C}$ is decreased from the right Hopf bifurcation point to the chaotic region, the stable cycles of one, two, three, and four periods arise, as shown in fig. 7. Here, the first column shows the time sequence of membrane potential, the second column that of intracellular calcium concentration, and the third column the trajectories of membrane potential vs. intracellular calcium. Note from the top row that $g^*_{K,C} = 27$ s^{-1} leads to a single pulse with a shape much different from and a period much longer than those of fig. 1. Also note that as $g^*_{K,C}$ decreases, the membrane potential bifurcates into doublet, triplet and bursting and finally to chaos. Holden et al. [33] and Holden and Winlow [34] have observed experimentally that a molluscan neuron also bifurcates into doublet, triplet and bursting discharges, and then through regular,

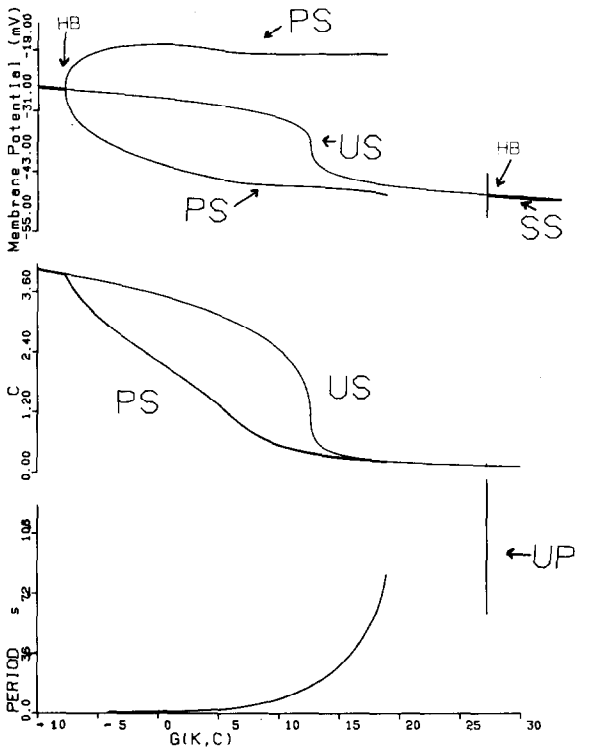

Fig. 6. Bifurcation diagram of the three-variable excitable cell using $g^*_{K,C}$ as a bifurcation parameter. From the top trace to the bottom, we show the membrane potential, intracellular calcium ion concentration, and period as a function of $g^*_{K,C}$, respectively. Here, HB stands for Hopf bifurcation point, SS for stable steady state, US for unstable steady state, and UP for unstable periodic state.

small amplitude oscillations to a depolarized steady state, in response to potassium channel inhibitors (e.g., TEA and 4AP). Note that the route to chaos seen here is quite different from the period doubling sequence shown in figs. 1–5, and has been also found in the cardiac cell membrane equations [17].

4. Conclusion

We have shown numerically that a three-variable model of an excitable cell can have endogeneous chaotic solutions, and that the chaos develops after a sequence of period doublings if a bifurcation parameter $g^*_{K,C}$ is increased from the left Hopf bifurcation point, or a sequence of n periods if $g^*_{K,C}$ is decreased from the right Hopf bifurcation point. It should be pointed out that this is the first, simple, biophysically realistic model for a nerve cell that shows chaos and that the numerical results look similar to experimental results [29–31, 33–35]. The implications of this aperiodic deterministic chaos is that endogeneously active excitable cells (nerve cells, cardiac muscle fibers) may show chaotic activity.

Ritzenberg et al. [10] have reported evidence of period-doubling and other bifurcative behavior in the electrocardiogram of the noradrenaline-treated dog, when the driving frequency was increased above a critical value. Although arrhythmias in the heart may stem from a very complex nature of the network system, the fact that chaos can be generated from such a simple excitable cell model like the one presented here indicates that this phenomenon might be mathematically tractable. Identification of the nature of the chaotic signals can provide valuable insights into the cellular mechanisms of cardiac arrhythmias, neural disorders, and other disorders of excitable tissues.

Acknowledgements

I would like to thank Dr. Arun Holden at the University of Leeds for excellent suggestions and comments. I would also like to thank Dr. Young Seek Lee at the National Institutes of Health for helps on AUTO.

Appendix A

In this appendix we provide explicit forms for the steady state probability functions, m_∞, h_∞, and n_∞ and the relaxation time τ_n.

We assume that the voltage dependencies of these quantities take the same expressions as the original Hodgkin–Huxley equations [24] but V is shifted along voltage axis by 50, 50, and 30 mV,

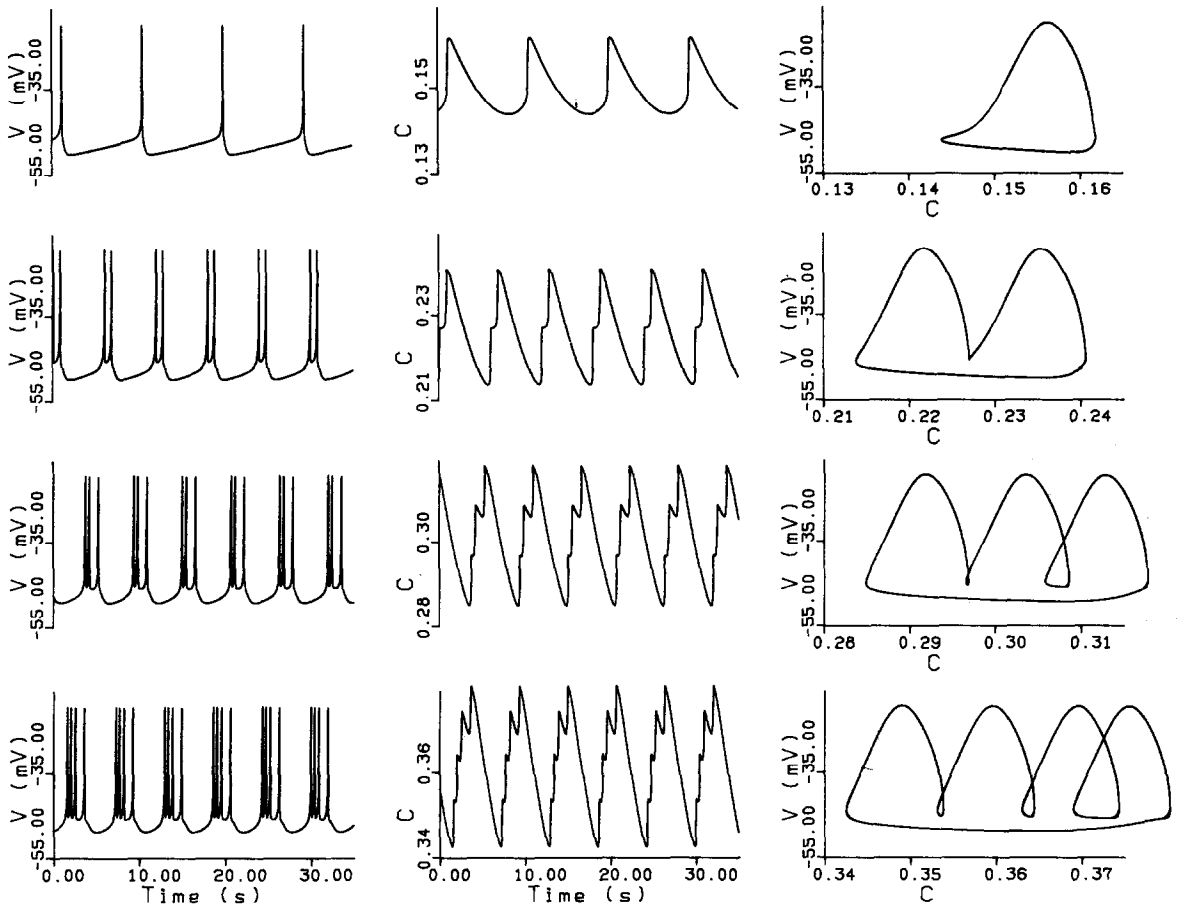

Fig. 7. The effect of decreasing $g^*_{K,C}$ from the right Hopf bifurcation point; i.e., $g^*_{K,C} = 27\ s^{-1}$, $19\ s^{-1}$, $15\ s^{-1}$, and $13\ s^{-1}$ from the top trace to the bottom. The left-hand column shows membrane potential (in mV) vs. time (in seconds), the middle column the intracellular calcium concentration vs. time (in s), and the right-hand column a limit cycle constructed using membrane potential and [Ca].

respectively. Thus,

$$y = \alpha_y/(\alpha_y + \beta_y), \tag{A.1}$$

where y stands for m_∞, h_∞, and n_∞, and

$$\alpha_m = 0.1(25 + V)/(1 - e^{-0.1V-2.5}), \tag{A.2}$$

$$\beta_m = 4e^{-(V+50)/18}, \tag{A.3}$$

$$\alpha_h = 0.07e^{-0.05V-2.5}, \tag{A.4}$$

$$\beta_h = 1/(1 + e^{-0.1V-2}), \tag{A.5}$$

$$\alpha_n = 0.01(20 + V)/(1 - e^{-0.1V-2}), \tag{A.6}$$

$$\beta_n = 0.125e^{-(V+30)/80}. \tag{A.7}$$

We also assume that the relaxation time τ_n in eq. (2) follows the expression similar to that of Hodgkin and Huxley [24]:

$$\tau_n = [230(\alpha_n + \beta_n)]^{-1}. \tag{A.8}$$

References

[1] R.M. May, Nature 261 (1976) 459.
[2] L.F. Olsen and H. Degn, Nature 267 (1977) 177.
[3] M.R. Guevara, L. Glass and A. Shrier, Science 214 (1981) 1350.

[4] R.H. Simoyi, A. Wolf (1982) and H.L. Swinney, Phys. Rev. Lett. 49 245.
[5] H. Hayashi, M. Nakao and K. Hirakawa, Phys. Lett. A 88 (1982) 265.
[6] I.R. Epstein, K. Kustin, P. De Kepper and M. Orban, Sci. Am. 248 (1983) 112.
[7] A. Wolf, Nature 305 (1983) 182.
[8] A.V. Holden, Nature 305 (1983) 183.
[9] A.V. Holden and M.A. Muhamad, J. Electrophysiol. Tech. 11 (1984) 135.
[10] A.L. Ritzenberg, D.R. Adam and R.J. Cohen, Nature 307 (1984) 159.
[11] K.I. Agladze, V.I. Krinsky and A.M. Pertsov, Nature 308 (1984) 834.
[12] A.M. Saperstein, Nature 309 (1984) 303.
[13] T.R. Chay and Y.S. Lee, Biophys. J. 45 (1984) 841.
[14] T.R. Chay, Biol. Cybernetics 50 (1984) 301.
[15] R. King, J.D. Brachas and B.A. Huberman, Proc. Natl. Acad. Sci. (USA) 81 (1984) 1244.
[16] T.R. Chay and J. Rinzel, Biophys. J., March, 1985.
[17] T.R. Chay and Y.S. Lee, Biophys. J., in press. (1985).
[18] R.E. Plant, J. Math. Biol. 11 (1981) 15.
[19] T.R. Chay, J. Phys. Chem. 87 (1983) 2935.
[20] T.R. Chay and J. Keizer, Biophys. J. 42 (1983) 181.
[21] I. Atwater, C.M. Dawson, A. Scott, G. Eddlestone and E. Rojas, in: Biochemistry Biophysics of the Pancreatic β-cell (Thieme, New York, 1980), pp. 100–107.
[22] R.W. Meech, J. Exp. Biol. 81 (1979) 93.
[23] S.H. Thompson, J. Physiol. (London) 265 (1977) 465.
[24] J.A. Connor and C.F. Stevens, J. Physiol. (London) 213 (1971) 31.
[25] D. DiFrancesco and D. Noble, in: Cardiac Rate and Rhythm, L.N. Bouman and H.J. Jongsma, eds. (Nijhoff, The Hague, 1982), pp. 93–128.
[26] A. Hodgkin and A. F. Huxley, J. Physiol. (London) 117 (1952) 500.
[27] J. Rinzel, The American Physiological Society of the 68th Annual Meeting of the Federation of American Societies for Experimental Biology, in press. (1985).
[28] A.L.F. Gorman and M.V. Thomas, J. Physiol. (London) 275 (1978), 357.
[29] E. Labos and E. Lang, in: Abnormal Neuronal Discharges, N. Chalazontis and M. Boisson, eds. (Raven, New York, 1978), pp. 177–188.
[30] J. Hoyer, M.R. Park and M.R. Klee, in: Abnormal Neuronal Discharges, N. Chalazontis and M. Boisson, eds. (Raven, New York, 1978), pp. 301–310.
[31] M.R. Klee, D.S. Faber and J. Hoyer, in: Abnormal Neuronal Discharges, N. Chalazontis and M. Boisson, eds. (Raven, New York, 1978), pp. 287–299.
[32] E. Doedel, Cong. Num. 30 (1981) 265.
[33] A.V. Holden, W. Winlow and P.G. Haydon, Comp. Biochem. Physiol. 73A (1982), 303.
[34] A.V. Holden and W. Winlow, Biol. Cybern 42 (1982) 169, 189.
[35] P.R. Benjamin, in: Abnormal Neuronal Discharges, N. Chalazontis and M. Boisson, eds. (Raven, New York, 1978), pp. 205–216.